AMS Home   Journals Home   Journal Archive   Subscribe   For Authors   Help   Advanced Search   Search   Go

Full Text View

A Model for Vortex-Trapped Internal Waves

Eric Kunze and Emmanuel Boss[*]

School of Oceanography, University of Washington, Seattle, Washington

ABSTRACT

Regions of negative vorticity are observed to trap and amplify near-inertial internal waves, which are sources of turbulent mixing 10–100 times higher than typically found in the stratified ocean interior. Because these regions are of finite lateral extent, trapped waves will not form a continuum but be quantized in modes. A model for the radial structure of near-inertial azimuthal modes in an axisymmetric vortex is described in order to explain intense near-inertial motions observed in the cores of a Gulf Stream warm-core ring and a vortex cap above Fieberling Seamount. Observed signals exhibit little variability of the rectilinear phase $\Phi = \arctan(\upsilon/u)$ in the core and evanesce rapidly outside the swirl velocity maximum, where u is the zonal velocity and υ the meridional velocity. The authors focus on azimuthal mode $n = -1$ (propagating clockwise around the vortex) and the gravest radial mode (no zero crossing) that appears to dominate observations. Model solutions resemble Bessel functions inside the velocity maximum and modified Bessel function decay outside, consistent with observations and solutions previously found by Kunze et al. using a less complete model. The improved model supports their conclusions concerning radial wavelengths, vertical group velocities, and energy fluxes for trapped waves.

Options:
- Create Reference
- Email this Article
- Add to MyArchive
- Search AMS Glossary

Search CrossRef for:
- Articles Citing This Article

Search Google Scholar for:
- Eric Kunze
- Emmanuel Boss

1. Introduction

Relative vorticity ζ associated with rectilinear geostrophic currents modulates the lower bound of the internal-wave frequency band to an effective Coriolis frequency, about $f + \zeta/2$ (Healy and LeBlond 1969; Mooers 1975; Kunze 1985; Young and Ben Jelloul 1997), where f is the planetary Coriolis frequency. Magaard (1968) was first to note that meridionally sheared zonal flow $U(y)$ can shift the turning latitude for a given frequency. In regions of anticyclonic vorticity ($\zeta < 0$), the internal waveband is broadened, allowing near-inertial waves with intrinsic frequencies below the planetary Coriolis frequency f. Because negative vorticity regions are of finite lateral extent, trapped waves will not form a continuum but will be quantized in discrete horizontal modes.

In this note, we describe gravest radial mode solutions for near-inertial waves trapped in a steady axisymmetric anticyclonic vortex. Because of the axisymmetric geometry, azimuthal and radial wavenumbers will be quantized while vertical wavenumber can be continuous. In an axisymmetric vortex, we find trapped modes in the frequency band $f + \zeta <$

$\omega_i < f + \zeta/2$ in contrast to the $f + \zeta/2 < \omega_i < f$ trapping band found in rectilinear flow (Kunze 1985).

This model is an attempt to explain the properties of intense near-inertial motions observed in the negative vorticity cores of a vortex cap found atop Fieberling Seamount (Kunze and Toole 1997) and a Gulf Stream warm-core ring (Kunze et al. 1995). The seamount measurements were intended to describe the response of an isolated peak to ambient motions. They revealed a 200-m-thick vortex of core vorticity $-0.5f$ above the summit within which there was turbulence 100 times more intense than typically found in the main pycnocline, and slightly subinertial motions. This range of time and space scales was driven by the barotropic diurnal tides (see also Eriksen 1991; Brink 1995). The warm ring measurements were designed to evaluate turbulence and mean-flow energy sinks for near-inertial motions at a near-inertial critical layer. Intensified near-inertial motions found at the base of the ring's core were probably generated by the passage of atmospheric storms (D'Asaro 1985).

Inside the cores of these vortices, observed near-inertial motions exhibited little variability in rectilinear horizontal phase ϕ = arctan($\mathbf{v}/u$), where u and $\mathbf{v}$ are the zonal and meridional near-inertial velocities. Outside the core, they evanesced rapidly. An absence of rectilinear phase progression is also found in numerical simulations of impulsively wind-forced warm-core rings (J. F. Price 1997, personal communication). Lack of rectilinear phase progression is not consistent with propagating plane waves. It can, however, be interpreted as azimuthal propagation in cylindrical coordinates since azimuthally invariant Cartesian u and $\mathbf{v}$ imply radial velocity $u_r = u \cos\theta + \mathbf{v} \sin\theta$ and azimuthal velocity $\mathbf{v}_\theta = \mathbf{v} \cos\theta - u \sin\theta$, where θ is the azimuthal angle.

A model for the gravest radial mode structure of a vortex-trapped near-inertial internal wave was previously presented in the appendix of Kunze et al. (1995). However, there are a number of errors in their approach. These include (i) neglect of regular singularities in the coefficients and (ii) neglect of interactions with mean-flow confluence $V_\theta/r - \partial V_\theta/\partial r$ outside the velocity maximum. Kunze et al. (1995) also incorrectly matched radial velocity u_r and its derivative $\partial u_r/\partial r$ across the velocity maximum rather than the more appropriate u_r and pressure p. In this note, we correct these errors. For the oceanic range of parameter values (Tables 1 and 2), the solutions resemble the Kunze et al. (1995) predictions, that is, Bessel functions inside the core and decaying modified Bessel functions outside.

The equation of motion for radially trapped near-inertial modes in an axisymmetric anticyclonic vortex is formulated in section 2. A model vortex described in section 3 is used to specify the equations further in section 4. Then, in section 5, we seek the gravest radial mode solution for this vortex. In section 6, its structure is compared with observations and the approximate model in the appendix of Kunze et al. (1995) and the trapped-wave dispersion relation is described.

2. Equations of motion

Following Kunze et al. (1995), consider near-inertial (hydrostatic, $\omega \ll N$) internal oscillations in a tall steady axisymmetric vortex with azimuthal velocity $V_\theta(r, z)$. The inertial oscillations are assumed to have a wave solution of the form $\psi = \psi_o(r) \cdot \exp[i(n\theta + k_z z - \omega_E t)]$, where n is the azimuthal mode number, $k_z = 2\pi/\lambda_z$ the vertical wavenumber, ω_E the invariant Eulerian frequency, and ω_i the intrinsic (Lagrangian) frequency following the mean flow; so motion is wavelike in azimuth, depth, and time. The r-dependent intrinsic frequency can be obtained from the substantial derivative $-i\omega_i = D/Dt = \partial/\partial t + (V_\theta/r)\partial/\partial\theta = -i(\omega_E - nV_\theta/r)$. The equations of motion linearized about the background flow reduce to

$$-i\omega_i u_r - \left[f + \frac{2V_\theta}{r}\right]v_\theta = -\frac{\partial p}{\partial r}$$

$$-i\omega_i v_\theta + \left[f + \frac{V_\theta}{r} + \frac{\partial V_\theta}{\partial r}\right]u_r = -\frac{inp}{r}$$

$$0 = -ik_z p + b \Rightarrow p = -\frac{ib}{k_z} = -\frac{N^2 w}{\omega_i k_z}$$

$$-i\omega_i b + N^2 w = 0 \Rightarrow b = -\frac{iN^2 w}{\omega_i}$$

$$\frac{1}{r}\frac{\partial(ru_r)}{\partial r} + \frac{inv_\theta}{r} + ik_z w = 0, \tag{1}$$

where (u_r, v_θ, w) are the radial, azimuthal, and vertical velocities; $b = -N^2\xi$ the wave buoyancy anomaly; ξ the vertical

displacement (positive upward); p the wave perturbation reduced pressure; and B the vortex plus background buoyancy. We assume vortex Burger number (aspect ratio) $R_L = (NH/fL)^2 = \{N\sqrt{/[f(\partial V_\theta/\partial z)]}\}^2 \gg 1$ so that interaction terms involving mean vertical shear $\partial V_\theta/\partial z$, mean radial buoyancy gradient $\partial B/\partial r = (f + 4V_\theta/r)\partial V_\theta/\partial z$, and the radial gradient in buoyancy frequency $\partial N^2/\partial r = \partial^2 B/\partial z\partial r$ can be neglected. In both the Gulf Stream warm-core ring and the Fieberling Seamount vortex cap, length scale Burger numbers R_L are $O(1)$ (Tables 1 ⊙ and 2 ⊙). However, $\partial N^2/\partial r$ is negligible in the Fieberling vortex and would result in at most 14% errors in the warm ring because their vorticities are $O(-f)$ (see end of section 6).

Eliminating reduced pressure p and buoyancy $b = -N^2\xi$, assuming that the buoyancy frequency N depends only weakly on radius and noting that

$$\frac{\partial \omega_i}{\partial r} = \frac{n}{r}\left[\frac{V_\theta}{r} - \frac{\partial V_\theta}{\partial r}\right]$$

$$\frac{\partial p}{\partial r} = -\frac{N^2}{\omega_i k_z}\frac{\partial w}{\partial r} + \frac{nN^2}{\omega_i^2 k_z r}\left[\frac{V_\theta}{r} - \frac{\partial V_\theta}{\partial r}\right]w, \qquad (2)$$

allows (1) to be reduced to three equations:

$$-i\omega_i u_r - \left[f + \frac{2V_\theta}{r}\right]v_\theta = \frac{N^2}{\omega_i k_z}\frac{\partial w}{\partial r} - \frac{nN^2}{\omega_i^2 k_z r}\left[\frac{V_\theta}{r} - \frac{\partial V_\theta}{\partial r}\right]w$$

$$-i\omega_i v_\theta + \left[f + \frac{V_\theta}{r} + \frac{\partial V_\theta}{\partial r}\right]u_r = i\frac{nN^2\cdot w}{\omega_i k_z r}$$

$$\frac{1}{r}\frac{\partial(ru_r)}{\partial r} + \frac{inv_\theta}{r} + ik_z w = 0. \qquad (3)$$

From the azimuthal momentum equation, one can isolate the azimuthal velocity

$$v_\theta = -i\left[\frac{f + V_\theta/r + \partial V_\theta/\partial r}{\omega_i}\right]u_r - \frac{nN^2}{\omega_i^2 k_z r}w \qquad (4)$$

so that it can be eliminated from the radial momentum equation:

$$-i\omega_i k_z r[\omega_i^2 - (f + \zeta + \chi)(f + \zeta)]u_r$$

$$= N^2\omega_i r\frac{\partial w}{\partial r} - nN^2[f + \zeta + 2\chi]\cdot w, \qquad (5)$$

where the vorticity $\zeta = V_\theta/r + \partial V_\theta/\partial r$ and the confluence $\chi = V_\theta/r - \partial V_\theta/\partial r$, and from continuity to isolate the vertical velocity

$$w = -i\left[\frac{\omega_i^2 k_z r}{n^2 N^2 - \omega_i^2 k_z^2 r^2}\right]\frac{\partial(ru_r)}{\partial r}$$

$$- i\left[\frac{n(f + \zeta)\omega_i k_z}{n^2 N^2 - \omega_i^2 k_z^2 r^2}\right](ru_r). \qquad (6)$$

Substituting (6) into (4), we can express the azimuthal velocity v_θ in terms of the radial velocity u_r

$$v_\theta = \frac{inN^2}{n^2 N^2 - \omega_i^2 k_z^2 r^2}\frac{\partial(ru_r)}{r} + \frac{i(f + \zeta)\omega_i k_z^2 r^2}{n^2 N^2 - \omega_i^2 k_z^2 r^2}u_r,$$

and from (6) and (1), the remaining consistency relations for buoyancy b and pressure p are

$$b = -\frac{N^2\omega_i k_z r}{n^2N^2 - \omega_i^2 k_z^2 r^2}\frac{\partial(ru_r)}{\partial r} + \frac{n(f + \zeta)N^2 k_z r}{n^2N^2 - \omega_i^2 k_z^2 r^2}u_r,$$

$$p = \frac{iN^2\omega_i r}{n^2N^2 - \omega_i^2 k_z^2 r^2}\frac{\partial(ru_r)}{\partial r} + \frac{in(f + \zeta)N^2 r}{n^2N^2 - \omega_i^2 k_z^2 r^2}u_r.$$

Vertical velocity w (6) has radial derivative

$$\frac{\partial w}{\partial r} = -\frac{i\omega_i^2 k_z r}{(n^2N^2 - \omega_i^2 k_z^2 r^2)}\frac{\partial^2(ru_r)}{\partial r} - \frac{i\omega_i k_z}{(n^2N^2 - \omega_i^2 k_z^2 r^2)}\left[(\omega_i + n(f + \zeta + 2\chi)) + \frac{2(\omega_i + n\chi)\omega_i^2 k_z^2 r^2}{(n^2N^2 - \omega_i^2 k_z^2 r^2)}\right]\frac{\partial(ru_r)}{\partial r}$$

$$- \frac{ink_z}{(n^2N^2 - \omega_i^2 k_z^2 r^2)}\left[\omega_i(r\partial^2 V_\theta/\partial r^2 - \chi) + n(f + \zeta)\chi + \frac{2(f + \zeta)(\omega_i + n\chi)\omega_i^2 k_z^2 r^2}{(n^2N^2 - \omega_i^2 k_z^2 r^2)}\right]u_r. \tag{7}$$

(Click the equation graphic to enlarge/reduce size)

Substituting for vertical velocity w and its radial derivative $\partial w/\partial r$ in the radial momentum equation,

$$0 = \frac{\partial^2 u_r}{\partial r^2} + \frac{1}{r}\left[3 + \frac{2\omega_i(\omega_i + n\chi)k_z^2 r^2}{(n^2N^2 - \omega_i^2 k_z^2 r^2)}\right]\frac{\partial u_r}{\partial r} + \left[\frac{[\omega_i^2 - (f + \zeta)(f + \zeta + \chi)]k_z^2}{N^2} - \frac{n^2 - 1}{r^2} + \frac{n(r\partial^2 V_\theta/\partial r^2 - \chi)}{\omega_i r^2}\right.$$

$$\left. + \frac{2(\omega_i + n(f + \zeta))(\omega_i + n\chi)k_z^2}{(n^2N^2 - \omega_i^2 k_z^2 r^2)}\right]u_r. \tag{8}$$

(Click the equation graphic to enlarge/reduce size)

3. Model vortex

Consider a steady axisymmetric vortex with a core of uniform negative vorticity ζ_0 inside radius r_0 and no annulus of positive vorticity outside the radius of maximum velocity r_0 as was approximately found for a Gulf Stream warm-core ring (Kunze et al. 1995) and for a vortex cap above Fieberling Seamount (Kunze and Toole 1997). The strength of this vortex could change in the vertical on scales larger than the near-inertial scale to satisfy the WKB approximation but here is taken to be barotropic to focus on the horizontal problem. The azimuthal velocity V_θ for such a vortex is described by

$$V_\theta = \begin{cases} \dfrac{\zeta_0 r}{2} & \text{for } r < r_0 \text{ (inside core)} \\ \dfrac{\zeta_0 r_0^2}{2r} & \text{for } r > r_0 \text{ (outside velocity max)} \end{cases} \tag{9}$$

(Fig. 1a ⊙⚊) so that the relative vorticity is

$$\zeta = \frac{V_\theta}{r} + \frac{\partial V_\theta}{\partial r} = \begin{cases} \zeta_0 & \text{for } r < r_0 \\ 0 & \text{for } r > r_0 \end{cases} \tag{10}$$

(Fig. 1b ⊙⚊), the confluence is

$$\chi = \frac{V_\theta}{r} - \frac{\partial V_\theta}{\partial r} = \begin{cases} 0 & \text{for } r < r_0 \\ \dfrac{\zeta_0 r_0^2}{r^3} & \text{for } r > r_0, \end{cases}$$

and the flow curvature with radius is

$$\frac{\partial^2 V_\theta}{\partial r^2} = \begin{cases} 0 & \text{for } r < r_0 \\ \dfrac{\zeta_0 r_0^2}{r^3} & \text{for } r > r_0 \end{cases} \tag{11}$$

4. Application

Application of vortex structure (9)–(11) to (8) and choosing azimuthal mode $n = -1$ to correspond to clockwise propagation around the vortex, consistent with the jetlike structure of trapped near-inertial oscillations in the warm-core ring (Kunze et al. 1995) and the Fieberling Seamount vortex cap (Kunze and Toole 1997), implies the following.

a. Inside the vortex core ($r < r_0$)

When the vorticity is uniform, (8) reduces to

$$0 = \frac{\partial^2 u_r}{\partial r^2} + \frac{1}{r}\left[\frac{3N^2 - \omega_i^2 k_z^2 r^2}{N^2 - \omega_i^2 k_z^2 r^2}\right]\frac{\partial u_r}{\partial r}$$

$$+ \frac{\omega_i^2 k_z^2}{N^2}\frac{(\omega_i - f_{\text{eff}})}{\omega_i}\left[\frac{\omega_i + f_{\text{eff}}}{\omega_i} + \frac{2N^2}{N^2 - \omega_i^2 k_z^2 r^2}\right]u_r,$$
$$\tag{12}$$

where the intrinsic frequency $\omega_i = \omega_E - nV_\theta/r = \omega_E + \zeta_0/2$ is invariant in the core if the core vorticity is constant, and $f_{\text{eff}} = f + \zeta_0$. Note that in an axisymmetric vortex, the lower bound of the internal wave band is broadened by ζ, while Kunze (1985) found broadening by only $\zeta/2$ in rectilinear shear. This difference is a result of the different geometries (see appendix B of Kunze 1985). Equation (12) is hyperbolic both inside and outside $r_1 = N/(\omega_i k_z)$. It *resembles* a Bessel equation but with singularities at $r_1 = N/(\omega_i k_z)$ in the coefficients of both $\partial u_r/\partial r$ and u_r.

b. Outside the velocity max ($r > r_0$)

Where vortex azimuthal velocity decays as $1/r$ outside the vortex core ($r > r_0$), (8) becomes

$$0 = \frac{\partial^2 u_r}{\partial r^2} + \frac{1}{r}\left[3 + \frac{2\omega_i(\omega_i - \zeta_0 r_0^2/r^2)k_z^2 r^2}{N^2 - \omega_i^2 k_z^2 r^2}\right]\frac{\partial u_r}{\partial r}$$

$$+ k_z^2\left[\frac{(\omega_i^2 - f(f + \zeta_0 r_0^2/r^2))}{N^2} + \frac{2(\omega_i - f)(\omega_i - \zeta_0 r_0^2/r^2)}{N^2 - \omega_i^2 k_z^2 r^2}\right]u_r, \tag{13}$$

where the intrinsic frequency $\omega_i = \omega_E - nV_\theta/r = \omega_E + \zeta_0 r_0^2/(2r^2) \rightarrow \omega_E$ as $r \rightarrow \infty$. Expressed in terms of the invariant Eulerian frequency ω_E, (13) can be expressed as

$$0 = \frac{\partial^2 u_r}{\partial r^2} + \frac{1}{r}\left[3 + \frac{2(\omega_E^2 r^4 - \zeta_0^2 r_0^4/4)k_z^2}{N^2 r^2 - \omega_E^2 k_z^2 r^4 - \omega_E \zeta_0 k_z^2 r_0^2 r^2 - \zeta_0^2 k_z^2 r_0^4/4}\right]\frac{\partial u_r}{\partial r}$$

$$+ k_z^2\left[\frac{(\omega_E^2 - f^2)r^4 + (\omega_E - f)\zeta_0 r_0^2 r^2 + \zeta_0^2 r_0^4/4}{N^2 r^4} + \frac{2((\omega_E - f)r^2 + \zeta_0 r_0^2/2)(\omega_E r^2 - \zeta_0 r_0^2/2)}{N^2 r^4 - \omega_E^2 k_z^2 r^6 - \omega_E \zeta_0 k_z^2 r_0^2 r^4 - \zeta_0^2 k_z^2 r_0^4 r^2/4}\right]u_r. \tag{14}$$

(Click the equation graphic to enlarge/reduce size)

For $r \gg r_0$ and $r \gg N/(\omega_E k_z)$, (14) reduces to

$$0 = \frac{\partial^2 u_r}{\partial r^2} + \frac{1}{r}\frac{\partial u_r}{\partial r} + \left[\frac{(\omega_E^2 - f^2)k_z^2}{N^2}\right]u_r. \tag{15}$$

For trapped waves ($\omega_E < f$), the lowest radial mode solution of (15) that vanishes at infinity is the radially decaying modified Bessel function $K_0(k_o r)$ with outer radial "wavenumber" $k_o = k_z(f^2 - \omega^2_E)^{1/2}/N$. For $r \gg k^{-1}_o$, $K_0(k_o r) \rightarrow \exp(-k_o r)/(r)^{1/2}$ so that $(\partial u_r/\partial r)/u_r \rightarrow -k_o$.

5. Method of solution

For the two oceanic examples (Tables 1 O= and 2 O=), r_1 lies inside the core ($r_1 < r_0$). Frobenius series expansions (appendix) about the regular singularities at $r = 0$ and $r = r_1 = N/(\omega_i k_z)$ in (12) are matched in u_r and $\partial u_r/\partial r$ at an intermediate point, for example, $r = r_1/2$, to provide a solution inside the core $r < r_0$.

Outside the core, (14) is mapped to a finite domain using $x = 1/r$

$$0 = \frac{\partial^2 u_r}{\partial x^2} - \frac{1}{x}\left[1 + \frac{2(\omega^2_E - \zeta^2_0 r^4_0 x^4/4)k^2_z}{N^2 x^2 - \omega^2_E k^2_z - \omega_E \zeta_0 k^2_z r^2_0 x^2 - \zeta_0 k^2_z r^4_0 x^4/4}\right]\frac{\partial u_r}{\partial x}$$
$$+ \frac{k^2_z}{x^4}\left[\frac{(\omega^2_E - f^2) + (\omega_E - f)\zeta_0 r^2_0 x^2 + \zeta^2_0 r^4_0 x^4/4}{N^2} + \frac{2x^2(\omega_E - f + \zeta_0 r^2_0 x^2/2)(\omega_E - \zeta_0 r^2_0 x^2/2)}{N^2 x^2 - \omega^2_E k^2_z - \omega_E \zeta_0 k^2_z r^2_0 x^2 - \zeta_0 k^2_z r^4_0 x^4/4}\right]u_r, \quad (16)$$

(Click the equation graphic to enlarge/reduce size)

which displays an irregular singularity at $x = 0$. We integrate from $x = 10^{-6}$ m^{-1}, where the modified Bessel function solution of (15) is used to relate u_r and $\partial u_r/\partial x$, via $(\partial u_r/\partial r)/u_r = -k_o$, to $x = 1/r_0$.

Inner and outer solutions for radial velocity u_r and pressure p are matched at $r = r_0$ for constant Eulerian frequency ω_E, azimuthal mode number $n = -1$, and vertical wavenumber k_z. The vorticity discontinuity $\Delta\zeta = \zeta_0$ at $r = r_0$ results in a discontinuity in the wave solution's radial derivative, $\Delta[\partial u_r/\partial r] = -u_r(r_0)\Delta\zeta/(\omega_i r_0)$. A compensating jump in azimuthal velocity $\Delta\upsilon_\theta$ ensures, through continuity (1), that vertical velocity w is smooth.

For comparison, Kunze et al. (1995) (i) neglected terms of the form $\zeta_0 r^2_0/r^2$ outside the core ($r > r_0$), (ii) approximated $N^2 - \omega^2_i k^2_z r^2$ as $-\omega^2_i k^2_z r^2$ throughout so that inner and outer solutions were Bessel functions $J_0(k_i r)$ and modified Bessel functions $K_0(k_o r)$, respectively, where k_i and k_o are inner and outer radial wavenumbers, and (iii) matched u_r and $\partial u_r/\partial r$ across $r = r_0$.

6. Results

Using properties found in a warm-core ring (Table 1 O=) and Fieberling Seamount's vortex cap (Table 2 O=), the range of gravest-radial-mode solutions (lower panels of Figs. 2 O= and 3 O=) are compared with Kunze et al.'s (1995) approximate Bessel solutions (upper panels). The solutions from the two approaches closely resemble each other.

The warm ring solutions (Fig. 2 O=) differ by at most a few percent. For warm ring properties (core radius $r_0 = 43$ km, core vorticity ζ between $-0.03f$ and $-0.1f$, and vertical wavelength $\lambda_z = 96$–200 m, Table 1 O=), the inner solution for $r < r_0$ closely resembles a lowest radial mode Bessel function $J_0(k_i r)$ (upper panel of Fig. 2 O=) with inner radial wavenumber $k_i = k_z(\omega^2_i - f^2_{eff})^{1/2}/N$. The trapped outer solution for $r > r_0$ (lower panel) closely resembles a modified Bessel function $K_0(k_o r)$ (upper panel) with outer radial wavenumber $k_o = k_z(f^2 - \omega^2_E)^{1/2}/N$. The solutions match smoothly across $r = r_0$. The inner radial wavelengths $\lambda_r = \lambda_i = 2\pi/k_i$, vertical group velocities Cg_z, and vertical energy-fluxes $Cg_z E$ found here agree quantitatively with those inferred by Kunze et al. (1995).

In the smaller, more intense vortex cap above Fieberling Seamount (core radius $r_0 = 5$–7 km, core vorticity ζ between $-0.45f$ and $-0.52f$, and wave vertical wavelengths $\lambda_z = 170$–220 m; Table 2 O=), the resemblence is less striking (Fig. 3 O=). The two solutions differ by the most (25%) at the core edge, $r = r_0$. As in the larger, weaker ring, the inner solution for $r < r_0$ (lower panel) resembles a Bessel function (upper panel) and the outer solution for $r > r_0$ (lower panel) a modified Bessel function (upper panel). Solutions are continuous but not smooth across $r = r_0$ because of the stronger vorticity discontinuity across the outer edge of the core. The solution best matching the observations (to within 15%) uses buoyancy frequency $N = 5.0 \times 10^{-3}$ s^{-1}, smaller core radius $r_0 = 5$ km, stronger core vorticity $\zeta = -0.52f$, and wave vertical

wavelength $\lambda_z = 170$ m. Possibly by coincidence, this solution has the Eulerian frequency closest (within 0.1%) to the K_1 diurnal frequency of the dominant tidal forcing. Its radial structure more closely resembles the observed structure than the Kunze et al. (1995) model in having a change in $\partial u_r / \partial r$ at $r = r_0 = 5$ km.

Figures 4 ⊙ and 5 ⊙ reveal that trapped-wave intrinsic frequencies are confined between the axisymmetric effective Coriolis frequency $f_{eff} = f + \zeta$ and $f + \zeta/2$. The vertical group velocity approaches zero at both extremes. At the low-frequency, low-aspect-ratio (small vertical wavelength) limit, the dispersion relation ω_i and vertical group velocity Cg_z have the same dependence on vertical wavelength λ_z as free internal waves, $\omega_i = (f^2_{eff} + N^2 k^2_i / k^2_z)^{1/2}$ (upper right panels) and $C_{g_z} = -(\omega^2_i - f^2_{eff})/(\omega_i k_z) \simeq -2(\omega_i - f_{eff})/k_z$ (lower right panels), respectively. More surprisingly, at the high-frequency limit ($\omega \lesssim f + \zeta/2$), aspect ratios are much larger for a given frequency than would be inferred from the free internal wave dispersion relation. That is, trapped waves ($\omega_i \lesssim f + \zeta/2$) exist for aspect ratios λ_z/λ_H corresponding to untrapped higher internal-wave frequencies ($\omega_i > f$). This arises because of the nonvanishing coefficient to $\partial u_r / \partial r$ and the second term in the coefficient to u_r in (12). For a given frequency, these allow higher aspect ratios than the free internal-wave dispersion relation.

In the ocean, the vertical wavelength λ_z, or aspect ratio λ_z/λ_r, will be limited by the vertical extent of the vortex. For the observed range of vertical wavelengths (stippling), the free internal-wave relation gives reasonable results in the warm-core ring (Fig. 4 ⊙) but overestimates the frequency and group velocity by a factor of 2 in the smaller, more intense vortex cap atop Fieberling Seamount (Fig. 5 ⊙).

We tested the consistency of neglecting the $\partial N^2/\partial r$ term by using our solution to estimate the size of neglected terms in the equation for u_r. In the Gulf Stream ring, the neglected term amounted to a maximum of 14% of the total near $r = r_0$. In the seamount vortex cap, $\partial N^2/\partial r$ vanished. Therefore, neglect of the $\partial N/\partial r$ term is justified in both cases.

7. Conclusions

Trapped near-inertial waves appear to be a common feature in anticyclonic vortices in the ocean, forced by astronomical tides over topographic features in the abyssal ocean and atmospheric storms in surface-intensified vortices. They are sources of turbulent mixing 10–100 times higher than typically found in the stratified ocean interior (Kunze et al. 1995; Kunze and Toole 1997).

A model for the gravest radial mode of near-inertial internal waves trapped in a steady axisymmetric vortex has been described and compared with observations in a Gulf Stream warm-core ring and a vortex cap atop Fieberling Seamount. Baroclinicity and critical layers have been ignored but could be treated in this model provided the vortex structure $V_\theta(r, z)$ is separable in radius r and depth z, the vortex Burger number $(NH/fL)^2$ is not too small, and the vortex's vertical scales exceed those of the wave so that the WKB approximation can be applied in the vertical. A more complete model would permit any length scale Burger number, strong radial variation of vortex buoyancy $B(r)$, more general radial structure $V_\theta(r)$ than assumed here, and nonseparable $V_\theta(r, z)$. The case where coefficient singularities in (8) lie outside the core $r_1 = N/(\omega_i k_z) > r_0$ (corresponding to large vertical wavelengths) might also be important in some circumstances.

Propagating wave structure was assumed in time, azimuth, and depth. The resulting dispersion relation is quantized in azimuthal and radial modes. We have assumed that vertical wavenumber and frequency are continuous, which requires that the vortex extend to infinity in the vertical or be bounded by an inertial critical layer as is common in the low- and midlatitude ocean. Only azimuthal mode $n = -1$ and radial mode zero were explored based on observed structure. Other modes might be of interest if evidence for them is found in the ocean. These would be generated by forcing on scales smaller than the vortex. In an analogous case of seamount-trapped wave generation about axisymmetric topography, Brink (1990) found generation of higher modes very inefficient compared to the gravest mode.

The vortex was assumed to have uniform vorticity in its core ($r < r_0$) and zero vorticity outside its velocity maximum ($r > r_0$). The vorticity discontinuity $\Delta\zeta$ results in discontinuities $\Delta(\partial u_r/\partial r)$ and $\Delta\upsilon_\theta$ at $r = r_0$. A continuous vorticity profile $\zeta(r)$ would produce smooth wave solutions. The radial structure for the gravest trapped radial mode resembles a Bessel function inside the vortex core (assumed to be of uniform vorticity) and modified Bessel function decay outside the velocity max (where the vorticity is assumed to vanish). Trapped frequencies are bound by $f_{eff} = f + \zeta < \omega_i < f + \zeta/2$ with vertical group velocity C_{g_z} vanishing at both extremes in vertical wavelength (aspect ratio). In the ocean, the frequency is likely to be imposed externally by the forcing and the horizontal scale set by that of the vortex. The vertical wavelength will then be fixed by the dispersion relation. For frequencies near the lower bound, $\omega_i \sim f + \zeta$ (smaller vertical wavelengths), the model's dispersion relation resembles that of free internal waves (Kunze et al. 1995). For frequencies near the upper bound, $\omega_i \sim f + \zeta/2$, the free internal-wave dispersion relation underestimates vertical wavelength and overestimates vertical group

velocity. The trapped wave's aspect ratio λ_z/λ_H is thus higher than it would be for free internal waves of the same ω_i and so has a broader range than would be expected for the range of trapped frequencies.

REFERENCES

Bender, C. M., and S. A. Orszag, 1978: *Advanced Mathematical Methods for Scientists and Engineers.* McGraw-Hill, 593 pp..

Brink, K. H., 1990: On the generation of seamount-trapped waves. *Deep-Sea Res.,* **37,** 1569–1582..

— ,1995: Tidal and lower frequency currents above Fieberling Guyot. *J. Geophys. Res.,* **100,** 10 817–10 832..

D'Asaro, E. A., 1985: The energy-flux from the wind to near-inertial motions in the surface mixed layer. *J. Phys. Oceanogr.,* **15,** 1043–1059..

Eriksen, C. C., 1991: Observations of amplified flows atop a large seamount. *J. Geophys. Res.,* **96,** 15 227–15 236..

Healey, D., and P. H. LeBlond, 1969: Internal wave propagation normal to a geostrophic current. *J. Mar. Res.,* **27,** 85–98..

Kunze, E., 1985: Near-inertial wave propagation in geostrophic shear. *J. Phys. Oceanogr.,* **15,** 544–565..

— ,and J. M. Toole, 1997: Tidally driven vorticity, diurnal shear and turbulence atop Fieberling Seamount. *J. Phys. Oceanogr.,* **27,** 2663–2693..

— ,R. W. Schmitt, and J. M. Toole, 1995: The energy balance in a warm-core ring's near-inertial critical layer. *J. Phys. Oceanogr.,* **25,** 942–957..

Magaard, L., 1968: Ein beitrag sur theorie der internen wellen as storungen geostrophischer stromungen. *Dtsch Hydrogr. Z.,* **21,** 241–278..

Mooers, C. N. K., 1975: Several effects of a baroclinic current on the cross-stream propagation of inertial–inertial waves. *Geophys. Fluid Dyn.,* **6,** 245–275..

Young, W. R., and M. Ben Jelloul, 1997: Propagation of near-inertial oscillations through a geostrophic flow. *J. Mar. Res.,* **55,** 735–766..

APPENDIX A

8. Frobenius Series Solutions

We solve <u>(12)</u> for $r < r_o$ in the case where the singularity $r_1 = N/(\omega_i k_z) < r_o$ using Frobenius series (<u>Bender and Orszag 1978</u>).

a. In the core: expanding about r = 0

Letting $y = u_r$ and $x = r/r_1$ where $r_1 = N/(\omega_i k_z)$, the equation in the vortex core <u>(12)</u> can be expressed as

$$
\begin{aligned}
0 = y'' &+ \frac{1}{x}\left[1 + \frac{2}{1 - x^2}\right]y' \\
&+ \left[\frac{\omega_i^2 - f_{\text{eff}}^2}{\omega_i^2} + \frac{2(\omega_i - f_{\text{eff}})}{\omega_i(1 - x^2)}\right]y.
\end{aligned} \qquad \text{(A1)}
$$

To find a Frobenius series solution about $x = 0$, we expand in terms of x

so that

$$y' = \sum_{n=0}^{\infty} a_n(n + \alpha)x^{(n+\alpha-1)},$$

$$y'' = \sum_{n=0}^{\infty} a_n(n + \alpha)(n + \alpha - 1)x^{(n+\alpha-2)}.$$

Noting that $1/(1 - x^2) = \sum_{m=0}^{\infty} x^{2m}$ and substituting into (A1) yields

$$0 = \sum_{n=0}^{\infty} \left[(n + \alpha)^2 a_n + 2 \sum_{m=0}^{n/2} (n - 2m + \alpha)a_{n-2m} \right] x^{(n+\alpha-2)}$$

$$+ \sum_{n=0}^{\infty} \left[\frac{\omega_i^2 - f_{\text{eff}}^2}{\omega_i^2} a_n + \frac{2(\omega_i - f_{\text{eff}})}{\omega_i} \sum_{m=0}^{n/2} a_{n-2m} \right] x^{(n+\alpha)}. \qquad (A2)$$

Setting $a_0 = 1$, the indicial equation is given by the equation for the coefficients of $x^{(\alpha+2)}$

$$\alpha^2 a_0 + 2\alpha a_0 = 0,$$

so that the indicial exponents are either $\alpha = -2$ or 0.

1) For $\alpha = -2$, power-series equation (A2) reduces to

$$0 = \sum_{n=0}^{\infty} \left[(n - 2)^2 a_n + 2 \sum_{m=0}^{n/2} (n - 2m - 2)a_{n-2m} \right] x^{(n-4)} + \sum_{n=0}^{\infty} \left[\frac{\omega_i^2 - f_{\text{eff}}^2}{\omega_i^2} a_n + \frac{2(\omega_i - f_{\text{eff}})}{\omega_i} \sum_{m=0}^{n/2} a_{n-2m} \right] x^{(n-2)}.$$

(Click the equation graphic to enlarge/reduce size)

The coefficients a_n are found by solving each successive equation in powers of x. We find for x^{-3}: $a_1 - 2a_1 = 0 \Rightarrow a_1 = 0$
and for x^{-2}

$$\left[\frac{\omega_i^2 - f_{\text{eff}}^2}{\omega_i^2} + \frac{2(\omega_i - f_{\text{eff}})}{\omega_i} - 4 \right] a_0 = 0.$$

This indicates that $a_0 = 0$ or the intrinsic frequency is strictly limited. Thus, the solution for $\alpha = -2$ is not physical.

2) The power series for $\alpha = 0$ in (A1) is the Taylor series:

$$0 = \sum_{n=0}^{\infty} \left[n^2 b_n + 2 \sum_{m=0}^{n/2} (n - 2m)b_{n-2m} \right] x^{(n-2)}$$

$$+ \sum_{n=0}^{\infty} \left[\frac{\omega_i^2 - f_{\text{eff}}^2}{\omega_i^2} b_n + \frac{2(\omega_i - f_{\text{eff}})}{\omega_i} \sum_{m=0}^{n/2} b_{n-2m} \right] x^n.$$

As before, the coefficients b_n can be solved for by gathering together like powers in x. For x^{-1}, we obtain $b_1 = 0$, for x^0,

$$b_2 = -\frac{1}{8} \left[\frac{\omega_i^2 - f_{\text{eff}}^2}{\omega_i^2} + \frac{2(\omega_i - f_{\text{eff}})}{\omega_i} \right]$$

and for $n > 2$, only even coefficients are nonzero

$$b_n = -\frac{1}{n(n+2)}\left[\frac{\omega_i^2 - f_{\text{eff}}^2}{\omega_i^2}b_{n-2} + 2\sum_{m=1}^{n/2}(n - 2m)b_{n-2m}\right.$$

$$+ \left.\frac{2(\omega_i - f_{\text{eff}})}{\omega_i}\sum_{m=0}^{(n-2)/2}b_{n-2m-2}\right].$$

Thus, around $x = 0$ and up to the singularity at r_1, the solution is $u = \Sigma\ b_n(r/r_1)^n$ with vanishing odd coefficients and even coefficients as given above.

b. In the core: Expanding about the singularity at $r = r_1 = N/(\omega_i k_z)$

To find Frobenius series solutions about $r = r_1$, (12) is rewritten letting $y = u_r$ and $x = (r - r_1)/r_1$, where $r_1 = N/(\omega_i k_z)$

$$0 = \frac{\partial^2 y}{\partial x^2} + \left[-\frac{1}{x} + \frac{3}{1 + x} - \frac{1}{2 + x}\right]\frac{\partial y}{\partial x}$$

$$+ \left[\frac{\omega_i^2 + f_{\text{eff}}^2}{\omega_i^2} - \frac{2(\omega_i - f_{\text{eff}})}{\omega_i x} + \frac{(\omega_i - f_{\text{eff}})}{\omega_i(2 + x)}\right]y.$$
$$(A3)$$

We expand

$$y = \sum_{n=0}^{\infty} c_n x^{(n+\alpha)}.$$

Noting that

$$\frac{1}{1 + x} = \sum_{m=0}^{\infty}(-1)^m x^m,$$

$$\frac{1}{2 + x} = \frac{1}{2}\frac{1}{1 + \dfrac{x}{2}} = \frac{1}{2}\sum_{m=0}^{\infty}\frac{(-1)^m x^m}{2^m},$$

and substituting these expressions back into (A3) yields

$$0 = \sum_{n=0}^{\infty}(n + \alpha)(n + \alpha - 2)c_n x^{(n+\alpha-2)} + \sum_{n=0}^{\infty}\left[-\frac{(\omega_i - f_{\text{eff}})c_n}{\omega_i} + \sum_{m=0}^{n}\left[3 - \frac{1}{2^{m+1}}\right](-1)^m(n - m + \alpha)c_{n-m}\right]x^{(n+\alpha-1)}$$

$$+ \sum_{n=0}^{\infty}\left[\frac{(\omega_i^2 - f_{\text{eff}}^2)c_n}{\omega_i^2} + \frac{(\omega_i - f_{\text{eff}})}{2\omega_i}\sum_{m=0}^{n}\frac{(-1)^m c_{n-m}}{2^m}\right]x^{(n+\alpha)}.$$
$$(A4)$$

(Click the equation graphic to enlarge/reduce size)

Setting $c_0 = 1$, the indicial equation is given by the coefficient of the lowest power in x, $x^{(\alpha-2)}$, yielding $\alpha(\alpha - 2) = 0$. Therefore, the inidicial exponents are either $\alpha = 0$ or 2.

1) For $\alpha = 0$, power series (A4) becomes

$$\sum_{n=0} \qquad \omega_i^2 \qquad\qquad 2\omega_i \qquad m=0 \qquad 2^m \qquad \Bigg]$$

with coefficients solved for by gathering like powers of x. For x^{-1}, we obtain

$$c_1 = -\frac{\omega_i - f_{\text{eff}}}{\omega_i},$$

while for x^0,

$$c_1 = -\frac{\omega_i - f_{\text{eff}}}{\omega_i}.$$

The coefficient c_2 is undefined so can be initialized independently [e.g., Case II(b)(ii) of Bender and Orszag (1978, p. 72)]. Without loss of generality, we set $c_2 = 0$. Changing it has no effect on the solutions, indicating that our numerical code is correct. Higher-order coefficients are given by

$$c_n = \frac{1}{n(n-2)}\Bigg\{\frac{(\omega_i - f_{\text{eff}})c_{n-1}}{\omega_i} - \frac{(\omega_i^2 - f_{\text{eff}}^2)c_{n-2}}{\omega_i^2}$$

$$- \sum_{m=0}^{n-1}\left[3 - \frac{1}{2^{m+1}}\right](-1)^m(n-m+1)c_{n-m-1} - \frac{\omega_i - f_{\text{eff}}}{2\omega_i}\sum_{m=0}^{n-2}\frac{(-1)^m c_{n-m-2}}{2^m}\Bigg\}.$$

2) The power series (A4) for $\alpha = 2$ is

$$0 = \sum_{n=0}^{\infty} n(n+2)d_n x^n + \sum_{n=0}^{\infty}\left[-\frac{(\omega_i - f_{\text{eff}})d_n}{\omega_i} + \sum_{m=0}^{n}\left[3 - \frac{1}{2^{m+1}}\right](-1)^m(n-m+2)d_{n-m}\right]x^{(n+1)}$$

$$+ \sum_{n=0}^{\infty}\left[\frac{(\omega_i^2 - f_{\text{eff}}^2)d_n}{\omega_i^2} + \frac{(\omega_i - f_{\text{eff}})}{2\omega_i}\sum_{m=0}^{n}\frac{(-1)^m d_{n-m}}{2^m}\right]x^{n+2}.$$

Coefficients d_n are obtained by gathering together like powers of x. For x^1,

$$d_1 = -\frac{5}{3} + \frac{(\omega_i - f_{\text{eff}})}{3\omega_i},$$

for x^2,

$$d_2 = \frac{1}{12}\left[\frac{2f_{\text{eff}}^2}{\omega_i^2} + \frac{6f_{\text{eff}}}{\omega_i} + 19\right],$$

and for x^n, $n \geq 2$,

$$d_n = \frac{1}{n(n+2)}\Bigg\{\frac{(\omega_i - f_{\text{eff}})d_{n-1}}{\omega_i} - \frac{(\omega_i^2 - f_{\text{eff}}^2)d_{n-2}}{\omega_i^2} - \sum_{m=0}^{n-1}\left[3 - \frac{1}{2^{m+1}}\right](-1)^m(n-m+1)d_{n-m-1}$$

$$- \frac{\omega_i - f_{\text{eff}}}{2\omega_i}\sum_{m=0}^{n-2}\frac{(-1)^m d_{n-m-2}}{2^m}\Bigg\}.$$

Thus, the solution u_r near r_1 is given by

$$u_r = A\sum c_n[(r - r_1)/r_1]^{(n+2)} + B\sum d_n[(r - r_1)/r_1]^n.$$

The series solutions for u_r and $\partial u_r/\partial r$ around $r = 0$ and $r = r_1 = N/(\omega_i k_z)$ are matched at a point between $r = 0$ and $r = r_1$, for example, $r = r_1/2$. This sets the magnitude of the series expansion around $r = r_1$ in terms of the amplitude at $r = 0$.

Tables

Table 1. Background, ring, and near-inertial wave properties observed in the WRINCL Gulf Stream warm-core ring (Kunze et al. 1995).

|	
N	$(4.5–5.1) \times 10^{-3}$ s^{-1}
f	9.4×10^{-5} rad s^{-1}
r_0	43×10^3 m
H	700 m
R_L	0.6–0.8
core ζ_0	$-(0.38–0.94) \times 10^{-5}$ s^{-1}
λ_z	96–200 m
k_z	$(3.1–6.5) \times 10^{-2}$ m^{-1}

Click on thumbnail for full-sized image.

Table 2. Background, vortex, and near-inertial wave properties observed in the vortex cap above Fieberling Seamount (Kunze and Toole 1997).

|	
N	$(4–5) \times 10^{-3}$ rad s^{-1}
f	8.0×10^{-5} rad s^{-1}
r_0	$(5–7) \times 10^3$ m
H	200 m
R_L	2.0–6.5
core ζ_0	$-(3.6–4.2) \times 10^{-3}$ s^{-1}
λ_z	170–220 m
k_z	$(2.9–3.7) \times 10^{-2}$ rad m^{-1}
ω_g	$K_1 = 0.933f = 7.5 \times 10^{-5}$ s^{-1}
core ω_i	5.5×10^{-5} s^{-1}
$r_1 = N/\omega_i k_z$	3.3×10^3 m

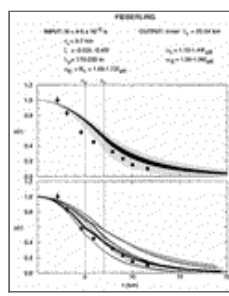Click on thumbnail for full-sized image.

Figures
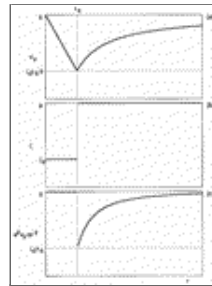
Click on thumbnail for full-sized image.

Fig. 1. Model vortex radial structure (9)–(11). Panels show azimuthal velocity V_θ (a), vorticity $\zeta = V_\theta/r + \partial V_\theta/\partial r$ (b), and flow curvature $\partial^2 V_\theta/\partial r^2$ (c). Model vorticity ζ (b) is uniform in the core ($r < r_0$) and vanishes outside the velocity maximum ($r > r_0$).
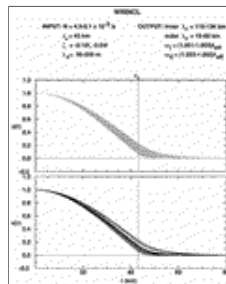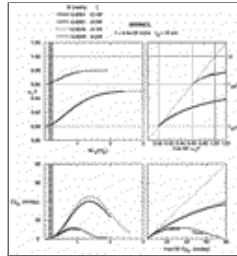

Click on thumbnail for full-sized image.

Fig. 2. Comparison of solution envelopes for properties found in a warm-core ring (Table 1 ⊙) reveals little difference between Kunze et al.'s approximate solution (upper panel) and the more rigorous one described here (lower panel). The gray envelope in the upper panel is the range of solutions given the observed range of buoyancy frequency N, core radius r_0, core vorticity ζ, and vertical wavelength λ_z (Table 1 ⊙). Radial wavelength is estimated from the free internal wave dispersion relation $\lambda_r = \lambda_z N/(\omega^2_i - f^2_{\text{eff}})^{1/2}$, which will overestimate λ_r at higher frequencies (Figs. 4 ⊙ and 5 ⊙). The inner solution to (12) for $r < r_0$ (lower panel) closely resembles a Bessel function (upper panel) though slightly flatter. The outer solution to (14) for $r > r_0$ (lower panel) closely resembles a modified Bessel function (upper panel). The solutions match smoothly across $r = r_0$. This supports the interpretation of Kunze et al. (1995) both qualitatively and quantitatively.

Fig. 3. Comparison of the radial structure for a gravest azimithal-mode-one vortex-trapped wave with observations (●) in a vortex cap over Fieberling Seamount. The gray envelope in the upper panel is the range of solutions given the observed range of buoyancy frequency N, core radius r_0, core vorticity ζ, and vertical wavelength λ_z (Table 2 ⊖) using the less accurate model presented in the appendix of Kunze et al. (1995). The black envelope further constrains the wave to have K_1 diurnal Eulerian frequency. The lower panel shows solutions for the observed range of N, r_0, ζ, and λ_z using the more rigorous model described in this paper. The two models' solutions resemble each other but radial velocity u_r across r_0 is not smooth in the more rigorous model. The solution (thick solid curve) best matching the observations (●) corresponds to smaller buoyancy frequency $N = 5.0 \times 10^{-3}$ s^{-1}, smaller core radius $r_0 = 5$ km, and stronger core vorticity $\zeta = -0.52f$. This solution has the closest (within 0.1%) Eulerian frequency to the K_1 diurnal frequency.

Fig. 4. Dispersion relations for vortex-trapped wave intrinsic frequency ω_i and vertical group velocity $Cg_z = \partial\omega_i/\partial k_z$ in the warm-core ring (Table 1 ⊖). Left panels display dependence on vertical wavelength λ_z. Right panels compare trapped-wave intrinsic frequency and vertical group velocity (vertical axes) with free "internal wave" solutions (horizontal axes) $\omega_i = (f^2_{\text{eff}} + N^2 k^2_i/k^2_z)^{1/2}$ (upper right panel) and $Cg_z \simeq -2(\omega_i - f_{\text{eff}})/k_z$ (lowering right panel). The two values of f_{eff} bracket the observed uncertainty in core vorticity (Table 1 ⊖). The free internal-wave dispersion relation overestimates trapped-wave frequencies and vertical group velocities at larger vertical wavelengths (higher aspect ratios). That is, trapped waves exist at aspect ratios that correspond to untrapped internal wave frequencies. For the observed range of vertical wavelengths (stippling), the free internal wave relation gives reasonable predictions.
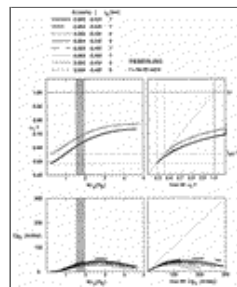
Fig. 5. Dispersion relation for vortex-trapped wave intrinsic frequency ω_i and vertical group velocity $Cg_z = \partial\omega_i/\partial k_z$ in Fieberling Seamount's vortex cap (Table 2 ⊖). Left panels display dependence on vertical wavelength λ_z. Right panels compare trapped-wave intrinsic frequency and vertical group velocity (vertical axes) with free "internal wave" relations (horizontal axes) $\omega_i = (f^2_{\text{eff}} + N^2 k^2_i/k^2_z)^{1/2}$ (upper right panel), and $Cg_z \simeq -2(\omega_i - f_{\text{eff}})/k_z$ (lower right panel). The two values of f_{eff} bracket the observed uncertainty in core vorticity (Table 2 ⊖). Free internal-wave vertical group velocities overestimate trapped group velocities by a factor of 2 in the observed range of vertical wavelengths (stippling).

* Current affiliation: College of Oceanic and Atmospheric Sciences, Oregon State University, Corvallis, Oregon.

Corresponding author address: Dr. Eric Kunze, School of Oceanography, University of Washington, Box 357940, Seattle, WA 98195-7940.

E-mail: kunze@ocean.washington.edu